Arabian Journal of Geosciences (2019) 12: 293
https://doi.org/10.1007/s12517-019-4387-z

REVIEW PAPER

Characteristics and controlling factors of the Lower–Middle Jurassic sandstone reservoirs in Amu Darya right bank area, Turkmenistan

Ting Zhang[1] · Jiajie Wu[1] · Huaiyi Fei[1]

Received: 9 February 2017 / Accepted: 22 February 2019 / Published online: 25 April 2019

Abstract

Based on laboratory analysis and core description, characteristics and the controlling factors of the Lower–Middle Jurassic reservoirs in Amu Darya right bank area are examined in this article. The study reveals that fine-grained lithic sandstones, feldspar–lithic sandstones, and siltstones are the main types of reservoir rocks in the central area, while fine-grained lithic–quartzose sandstones are predominant in the eastern area. The major pore types are intergranular and intragranular dissolved pores; the predominant pore throats are lamellar throats. Fractures develop poorly in the study region, but relatively well in the eastern area. The reservoirs are pore-dominated sandstone reservoirs with limited fractures, characterized by very low porosity and permeability. Reservoir evolution is jointly controlled by sedimentation, diagenesis, and tectonic movements. Sedimentation laid the foundation to porosity evolution. Subaqueous distributary channels and mouth bars are the beneficial lithofacies for reservoir development. Poor compressive strength of sandstones, deep paleoburial depth, and destructive subsidence style of the strata led to strong compaction. Primary pores are almost entirely destroyed by compaction and eogenetic calcite cementation. Ferroan dolomite cements and quartz overgrowths occupied the remaining intergranular pores furtherly. However, dissolution played an effective role on the generation of secondary pores, and the influences of authigenic clay minerals are minor on reservoirs. The Neogene–Quaternary tectonic movements caused intensive lateral compressional stress thus made further damage to reservoir pore structure. Nevertheless, fractures generated by tectonic movements increased reservoir permeability and provided valid migration pathways for the late dissolution fluids, therefore improved reservoir physical properties obviously.

Keywords Amu Darya · Lower–Middle Jurassic · Sandstone reservoir · Reservoir evolution

Introduction

Amu Darya Basin, situated in the eastern Turkmenistan and the southern Uzbekistan, is the most prolific and largest gas bearing basin in Central Asia (Fig. 1). More than 80% of natural gas reserves in Central Asia, representing approximately 3×10^{13} m^3, come from this basin (Henian et al. 2013). Amu Darya right bank area is located in the northeastern part of Amu Dara basin, and it is the joint development zone of China National Petroleum Company (CNPC) in Amu Darya Basin (Shikuo et al. 2013). Since 2007, comprehensive geological researches on Amu Darya right bank area have been carried out deeply, including stratigraphic classification, sedimentology, reservoir characteristics, and structural features. The Callovian–Oxfordian (Middle–Upper Jurassic) carbonate strata have been considered as the main gas producing layers for its reservoir characteristics. Numerous important achievements have been obtained on the Callovian–Oxfordian strata (e.g., Bing et al. 2010; Shilei et al. 2012; Qiang et al. 2013). However, concerning the Lower–Middle Jurassic strata best assigned to the lacustrine–deltaic depositional setting, previous studies were only focusing on hydrocarbon generation (e.g., Haowu et al. 2010), structural features (e.g., Shikuo et al. 2013), and sedimentology (Ting et al. 2014). This is because the Lower to Middle Jurassic is recognized as the main source rock interval with its organic-rich

Editorial handling: Roger Davies

Electronic supplementary material The online version of this article (https://doi.org/10.1007/s12517-019-4387-z) contains supplementary material, which is available to authorized users.

✉ Ting Zhang
zhangt_dyy@cnpc.com.cn

[1] Geologic Exploration & Development Research Institute, Chuanqing Drilling Engineering CO., Ltd., CNPC, No. 83, Block 1, Northern Jianshe Road, Chengdu 610051, Sichuan, China

Fig. 1 Geographical location map of Amu Darya Basin

mudstone zones. To date, very few researches aimed characterizing Lower to Middle Jurassic sandstones for their reservoir properties based on two wells (Well B××–21 and Well Y××–23)located in the central part of the Amu Darya right bank area (Hailiang et al. 2015).

Nonetheless, previous researches on terrigenous clastic strata in different regions in the world, including Permian System of Cooper Basin in Australia (Kewen 1986), Cretaceous Qingshankou Formation of the southern Songliao Basin in China (e.g., Mingda et al. 2003; Yu et al. 2010), and Eocene Liushagang Formation of Weixinan subbasin in south China sea (e.g., Baojia et al. 2011) reveal that sand bodies depositing in fluvial–deltaic and lacustrine settings may have great hydrocarbon potential, since they are interbedded with thick source rocks in large area and easy to accumulate oil and gas within small distance. Fluvial–deltaic and lacustrine strata are both proven to be source rock and reservoir intervals in Amu Darya. Before the exploration by CNPC, the former Soviet Union had discovered 16 gas fields with geological reserves more than 1 billion cubic meters in the Lower–Middle Jurassic strata in Amu Darya Basin during the last 50 years, and three of these gas fields are located in Amu Darya right bank area. The highest daily gas production was 1.6×10^4 m^3(Well S××–24 in Block A, tested in 1988). Therefore, the lacustrine and deltaic sandstone zones included within the thick Lower to Middle Jurassic organic-rich interval in Amu Darya have a high reservoir potential and therefore require more detailed research. Within the last 2 years, the regain of interest by the industry for Lower and Middle Jurassic clastic reservoirs was accompanied by drilling program and fieldwork campaigns in the course of which new rock samples have been acquired. In this study, we present new petrophysical data from Lower and Middle Jurassic continental deposits of the Amu Darya Basin. We aim to characterize the characteristics as well as the controlling factors of reservoirs in the whole study area.

Regional geological background

The Amu Darya Basin is located in the southeastern part of the Tulan platform and has an area of 420,000 km^2 (Wenli et al. 2012; Rongcai et al. 2013). The Amu Darya right bank area is situated between the Turkmenistan–Uzbekistan boundary and the Amu Darya River in the northeast of the basin (Fig. 2). It is divided into two blocks (Block A and B) according to the exploration phase. The total area of the study region is 14,314 km^2. Crossing the three main tectonic units of the basin, the Chardzhou terrace, the Beschkent depression, and the Gissar mountain subdivide the Amu Darya right bank area into five secondary tectonic units from northwest to southeast: (1) the Chardzhou Kenkyzkurt uplift, (2) the Karabek depression, (3) the Sandykly uplift, (4) the Beschkent depression, and (5) the Gissar uplift.

Based on tectonic and lithological characteristics, the Amu Darya basin is divided into three structural layers from the bottom to the top, including basement, intermediate layer, and sedimentary cover (Fig. 3). The basement is composed of the late Paleozoic igneous and metamorphic rocks which are strong-folded, and buried between 2000 m and 14,000 m. The intermediate layer above the basement consists of Permian–Triassic coarse clastic rocks and intermediate-acid extrusive rocks. The buried depth of this layer increases from north to south and reaches 12,000 m in the southwestern margin of the basin. The widely spread sedimentary cover is composed of Jurassic–Paleogene clastic, carbonate, and evaporite rocks (Wenli et al. 2012; Rongcai et al. 2013).

.The clastic-dominated Lower–Middle Jurassic corresponds to the bottom part of the Sedimentary Cover (Fig. 3). It disconformably overlies the Pernian–Triassic brown conglomerates belonging to the Intermediate Layer and is conformably overlaid by the Callovian–Oxfordian carbonate-dominated interval The thickness of the Lower–Middle Jurassic strata in Amu Darya Basin is mostly controlled by tectonism and the location of active faults during the time of deposition of the lacustrine/deltaic sediments.. In the study area, the strata decrease from southeast to northwest dramatically. The average strata thickness is more than 800 m in the eastern Block B, but decreases to less than 500 m in Block A, and reaches 0 m in the west part of the western Block B as a result of depositional break (Ting et al. 2014). As shown in Fig. 3, sandstone zones mainly ranging from 2~20 m are interbedded with thick dark mudstones in the strata. Besides, thin layers of carbargilite and coal bed as well as small amount of calcareous rocks are also developed (Fig. 3).

Materials and methods

The Lower–Middle Jurassic rock samples include cuttings from 12 wells and core data of 89 m from 4 wells. Reservoir sandstones were classified by following the nomenclature of sandstones proposed by Robert L. Folk in 1968 (Robert 1968; Xiaomin 2008) based on the clastic constituents, while were divided into four kinds based on the grain size according to the classification standard of grain size in National Standard of the People's Republic of China GB/T 17412.2-1998. The classification of pore–throat combination type follows the classification scheme proposed by Fengxiang Y in 1994 (Guohua et al. 2012).

Litholigical characteristic, pore spaces and diagenesis features of reservoirs were studied based on 25 thin sections stained with methylene blue method, as well as 66 SEM photomicrographs from 5 sample conducted by using JSM–5500LV scanning electron microscope. Both thin sections and SEM photomicrographs were undertaken by Key National Lab of Oil and Gas Reservoir Geology and Development Engineering, Chengdu University of Technology. Physical properties and mercury injection tests were conducted on cylinder shape samples (25 mm long and 25 mm in diameter), with CMS300 tester (Core Lab, Houston, TX, USA) for testing porosity and permeability under overburden pressure and AutoPore IV 9500 mercury injection apparatus (MICROMERRITICS INSTRUMENT CORP, Atlanta, GA, USA), in accordance with SY/T6385–1999 and SY/T 5346–1994, and undertaken by Key National Lab of Oil and Gas Reservoir Geology and Development Engineering, Chengdu University of Technology. Fluid inclusion homogenization temperature is measured by using THMSG 600 fluid inclusion analyzer, in accordance with SY/T5162–1997 and SY/T6189–

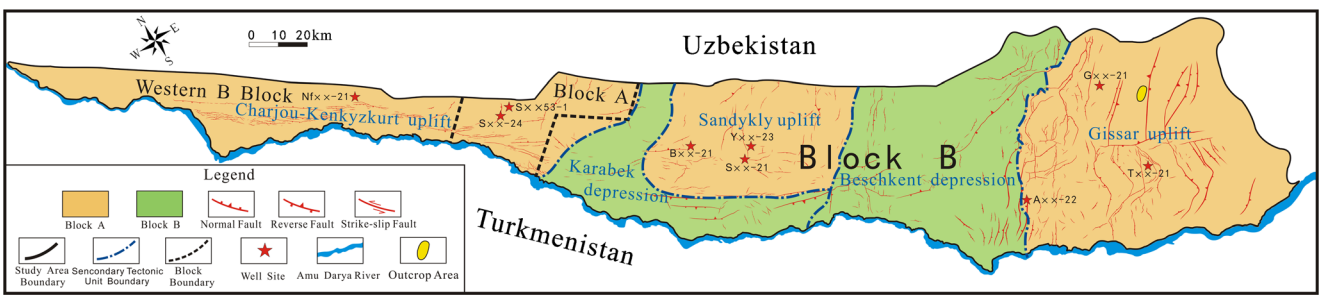

Fig. 2 Structural map of Lower–Middle Jurassic strata in Amu Darya right bank area

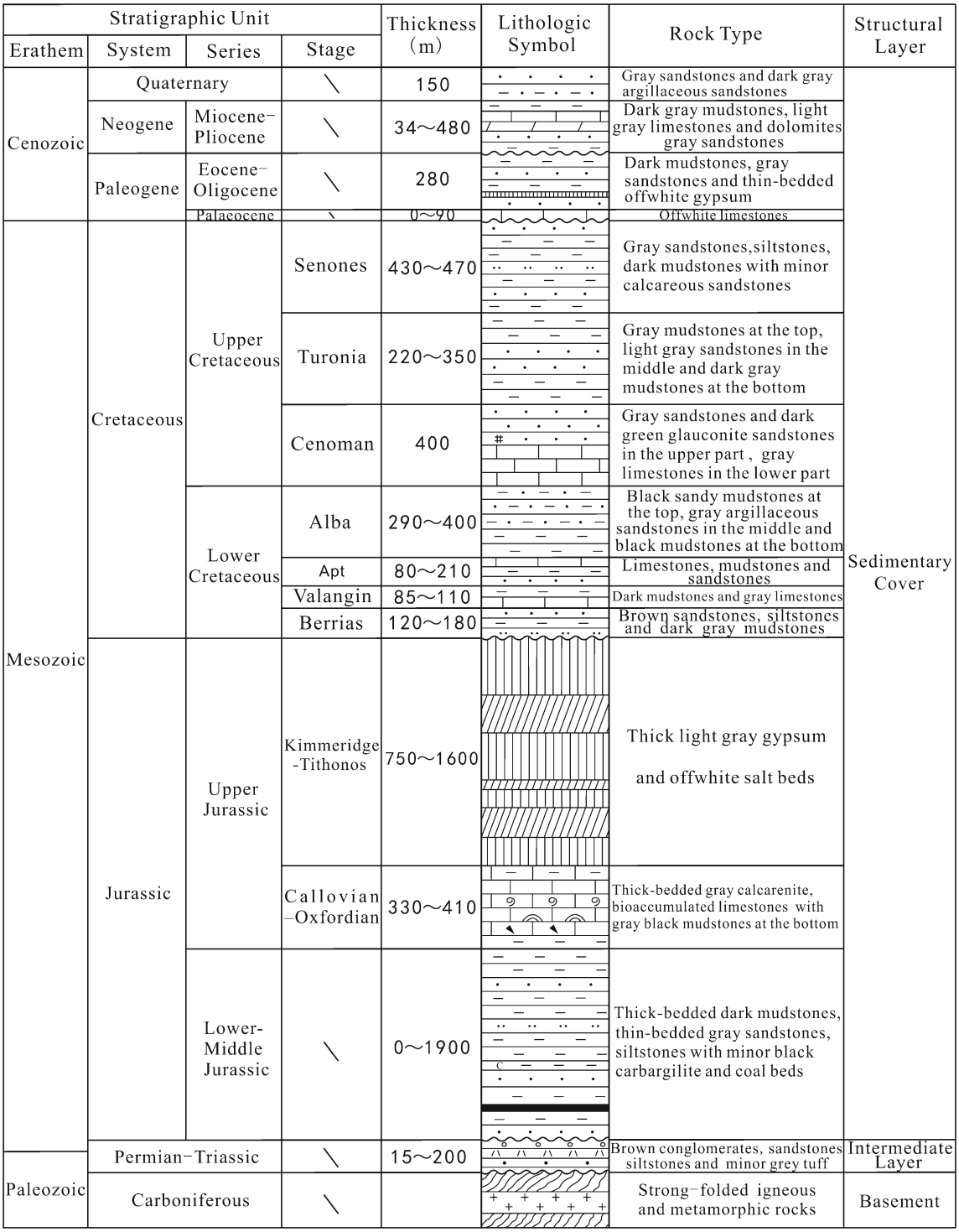

Fig. 3 Stratigraphic table of Amu Darya Basin

1996, and was undertaken by Institute of Geochemistry Chinese Academy of Sciences. All the detailed data are presented in Supplementary Table. FMI image processing and FMI data interpretation were undertaken by Schlumberger, and the data was processed with Schlumberger GeoFrame software version 4.5.

Characteristics of sedimentary facies

Previous studies on the Lower–Middle Jurassic sedimentary facies show that the strata consist predominantly of terrigenous clastic deposits with rare marine–continental transitional sediments at the top. Two transgressive sequences have been

recognized within the stratigraphy defining the lower and upper sections (Ting et al. 2014).

These four basic subfacies are recognized in the study area: delta front (freshwater), lakeshore (freshwater), shallow lake (freshwater), and subtidal zone (Table 1). The most common subfacies are lakeshore and shallow lake. Delta front subfacies are present predominantly in Block A and the eastern Block B, and develop primarily in the lower section of the strata and occasionally in the bottom of the upper section. Sedimentary facies associated with subtidal zone is preserved in limited area of the western and the eastern Block B in the top of the strata (Ting et al. 2014).

These four subfacies are subdivided into twelve lithofacies furtherly: subaqueous distributary channel, mouth bar, subaqueous natural levee, inter distributary bay, lakeshore mud, lakeshore swamp, lakeshore sand bar, shallow-lake mud, shallow-lake sand bank, mud flat, lime mud flat, and sand flat (Table 1). Among these lithofacies, lakeshore mud, lakeshore swamp, and shallow-lake mud lithofacies correspond to the organic-rich intervals, while the following four are of particular importance for reservoir characterization:

(1) Subaqueous distributary channel

Subaqueous distributary channel lithofacies alternate with interdistributary bay facies and develop on delta front facies in the study area. Typical sedimentary rocks present in this lithofacies are well-sorted from medium- to fine-grained sandstones. Coarse-grained sandstones are present occasionally. These sandstone bodies are usually lenticular and characterized by parallel beddings and current beddings with fining-upward pattern. Subaqueous distributary channels developed primarily during the Early Jurassic in the central and the eastern part of the study area (Ting et al. 2014).

(2) Mouth bar

Mouth bar lithofacies develop at the distal part of subaqueous distributary channels. This subfacies has characteristic of strong current and high sedimentation rate (Xiaomin 2008). According to drilling core analyses, the main sedimentary rocks associated with mouth bar in the study area are well-sorted from medium- to coarse-grained sandstones characterized by coarsening upward. Current beddings are common in mouth bar sandstones and the fossils are poor. The mouth bar subfacies was uncommon during the early and late time of the Early–Middle Jurassic in the central and eastern part of the study area. (Ting et al. 2014).

(3) Lakeshore sand bar

Lakeshore sand bar lithofacies alternate with mudstone-rich intervals in lakeshores (Xiaomin 2008). This lithofacies

Table 1 Types and lithology of sedimentary facies in Amu Darya right bank area

Facies	Subfacies	Lithofacies	Average thickness for individual interval	Lithology	Sedimentary structure
Delta (freshwater)	Delta Front	Subaqueous distributary channel	15.53	Grey, linen fine- to coarse-grained sandstones	Fining upward, parallel beddings, current beddings
		Mouth bar	5.32	Grey, medium- to coarse-grained sandstones	Coarsening upward, current bedding, cross bedding, plant fossils
		Subaqueous natural levee	8.02	Grey, linen siltstones, and argillaceous siltstones	Fining upward, current beddings
		Interdistributary bay	12.84	Dark grey mudstones and silty mudstones with minor siltstones and fine-grained sandstones bodies	Parallel beddings, horizontal bedding, troglobitic lebensspur
	Lakeshore	Lakeshore mud	19.20	Thick dark mudstones with minor dark carbargilites and dark grey silty mudstones	Horizontal bedding, raindrop imprint, bioturbation, plant fossils
	Lake	Lakeshore swamp	7.09	Dark coal bed and carbargilites	Plant fossils
		Lakeshore sand bar	8.21	Grey siltstones with minor silty mudstones and mudstones	Fining upward, lenticular beddings, current beddings
	Shallow Lake	Shallow-lake mud	60.12	Thick dark mudstones with minor carbargilites	Horizontal bedding, plant fossils
		Shallow-lake sand bank	6.22	Grey siltstones, argillaceous siltstones with minor fine-grained sandstones	Fining upward, lenticular beddings, diverse plant fossils
Tidal flat	Subtidal	Mud flat	20.03	Grey mudstones with lime mudstones	/
		Lime mud flat	35.39	Dark lime mudstones with minor dark grey argillaceous limestone	/
		Sand flat	5.57	Grey siltstone and argillaceous siltstone with minor fine-grained sandstones	Fining upward

is characterized by sheet-like or lenticular shape fine-grained sandstone and minor siltstone bodies. Lakeshore sand bar subfacies located in the study area is characterized by lenticular beddings, current beddings, and uncommon terrestrial plant debris. This lacustrine subenvironment is very common within the entire Lower–Middle Jurassic stratigraphic interval in the study area (Ting et al. 2014).

(4) Shallow-lake sand bank

Shallow-lake sand banks generally occur where the hydrodynamic force is generally weaker than the one located in the lakeshore areas (Xiaomin 2008). This lithofacies is primarily composed of siltstones and fine-grained sandstones. Shallow-lake sand banks are commonly interbedded with dark argillite-rich intervals and characterized by lenticular beddings and diverse plant fossils, such as Cladophlebis tongusorum Prynada. The shallow-lake sand bank was common during both the earlier and later stages of the Lower–Middle Jurassic based on the common occurrence of this subfacies type within the upper part the Lower to Middle Jurassic stratigraphic interval (Ting et al. 2014).

Reservoir characteristics

Lithological characteristics

Samples analyzed for this study include siltstones (Fig. 4a), fine-grained sandstones (Fig. 4b), medium-grained sandstones (Fig. 4c), and coarse-grained sandstones (Fig. 4d). Among them, fine-grained sandstone and siltstone are the most common types. Coarse- and medium-grained sandstones only present in subaqueous distributary channel and mouth bar lithofacies, and represent 12% of the reservoir rock volume in the strata (Table 2). The grain–size range is from 0.1 to 0.5 mm, with the maximum size being 0.7 mm (Fig. 4a–d). Common grains are moderately to well sorted, subangular to subrounded shape, and generally in long linear contacts to concave–convex contacts, which indicate a moderate degree of textural maturity and high degree of compaction.

Soft constituents include flaky minerals, claystone fragments, limestone fragments, and low-grade metamorphic lithic fragments and represent approximately 34% of the whole volume for both lithic– and feldspathic–lithic sandstones. The total proportion of hard constituents such as quartz, feldspar grains, and quartzose fragments is relatively low and only represents 45–50% (Table 3). The interstitial materials of lithic and feldspathic–lithic sandstones account for 21% and 13% of the whole rock volume, respectively. In comparison, the proportion of soft constituents is low and only represents 8% of the whole volume in lithic arkose, and the percentage of the total hard constituents is relatively high and go up to 68% (Table 3). Lithic–quartzose sandstones are poor in soft components (less than 9%), and rich in quartz grains and quartzose fragments (up to more than 72%). The percentage of interstitial materials of lithic–quartzose sandstones is less than 15% (Table 3).

Results indicate that the lithological composition of rock samples is most likely controlled by their spatial distribution and stratigraphic age. Lithic sandstones (53%) and feldspathic–lithic sandstones (41%) are the main rock types in Well Y××–23 and Well B××–21 which are located in the central Block B (Table 4). On the contrary, lithic–quartzose sandstones account for 48% and 37% of the whole rock type in Well G××–21 and Well T××–21, respectively; both wells are located in the eastern Block B (Table 4). Moreover, the percentage\ of lithic–quartzose sandstones is 52% of the rock type in the lower part of the section, and only about 10% in the upper part of the section (Table 4). In comparison, lithic– and feldspathic–lithic sandstones account for 38% in total in the lower section of the strata, and this percentage increases to 74% in the upper part of the section (Table 4). The data above indicate that the compositional maturity of the sandstones is generally low in the study area, especially in the central Block B and the upper section of the strata.

Physical properties of reservoir rocks

Analyses of thin sections and SEM photomicrographs indicate that the predominant pore spaces of the Lower–Middle Jurassic reservoirs are secondary porosity (Fig. 4b–f, Table 5), including intergranular dissolved pores (65%), intragranular dissolved pores (26%), and intercrystal pores (7%), since the primary pores (2%) are almost completely destroyed by diagenetic processes. Table 5 also reveals that intragranular dissolved pores are more common in the central Block B, while the proportion of residual primary pores increases slightly in the eastern Block B. The main range of pore diameter in reservoir sandstones is 30~280 μm, and the maximum size is up to about 700 μm (Table 5). To be specific, pore diameter of intragranular dissolved pores ranges primarily from 50 to 200 μm (Fig. 4c, d), while pore diameter of intergranular dissolved pores varies mainly from 40 to 280 μm (Fig. 4b, d, f), and pore diameter of intercrystal pores are generally less than 15 μm (Fig. 4e, f).

Based on the thin section observations and SEM photomicrographs, the predominant type of pore throats recognized in the strata is sheet-like lamellar throat which develop among grains and secondary crystals, and is commonly thin, narrow, short-extended (Fig. 4d, e). Besides, microfractures which crosscut grains and cements generated by compaction or tectonic movement are also effective pore throats in the study area, especially in the eastern Block B (Figs. 4d, 8d). According to the mercury injection measurement on Well B××–21 and Well Y××–21, the average coefficient of sorting

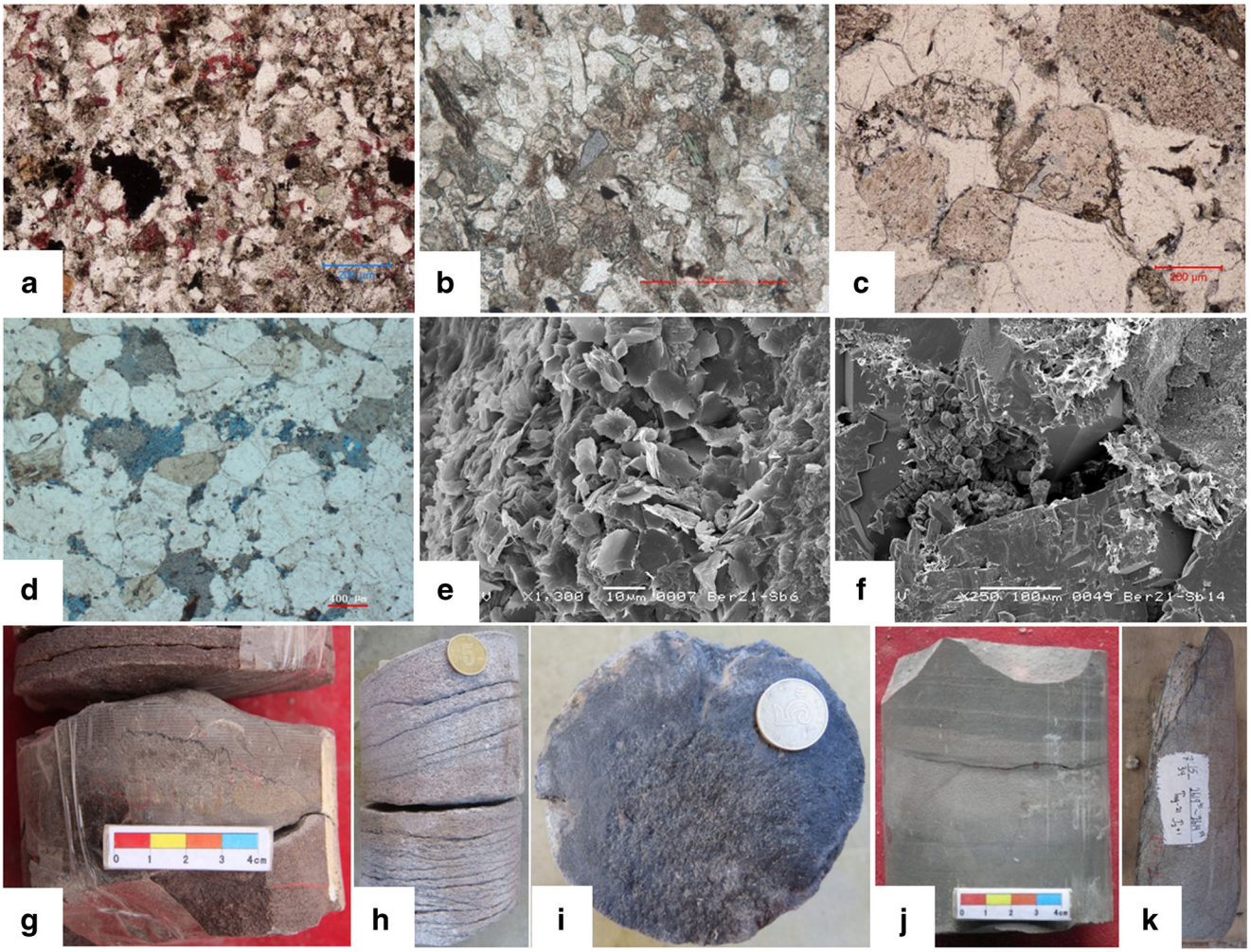

Fig. 4 Reservoir rocks and reservoir spaces of the Lower–Middle Jurassic in Amu Darya right bank area. **a** Siltstone, Well B××–21, 3281.50 m, scale bar represents 200 μm, plain light; b fine-grained lithic sandstone, Well Y××–23, 3812.80 m, scale bar represents 500 μm, plain light; **c** medium-grained feldspathic–lithic sandstone, with intragranular and intergranular dissolved pores, Well B××–21, 3284.10 m, scale bar represents 200 μm, plain light; **d** coarse-grained lithic–quartzose sandstone, with intergranular and intragranular dissolved pores, Well G××–21, 2892.72 m, scale bar represents 400 μm, plain light; **e** lamellar throats of kaolinite crystals, fine-grained feldspathic–lithic sandstone, Well B××–21, 3542.95 m, scale bar represents 20 μm, scanning electron microscope; **f** intercrystal and intergranular pores, fine-grained lithic–quartzose sandstone, Well B××–21, 3545.00 m, scale bar represents 100 μm, scanning electron microscope; **g** stylolite, fine-grained lithic–quartzose sandstone, Well B××–21, 3542.88~3542.99 m, drilling core; **h** laminae fractures, coarse-grained lithic–quartzose sandstone, Well G××–21, 2890.99~2891.13 m, drilling core; **i** asphalt on laminae fracture surface, coarse-grained lithic–quartzose sandstone, Well G××–21, 2889.73m, drilling core; **j** laminae fractures, fine-grained lithic sandstone, Well Y××–23, 3815.62~3815.75 m, drilling core; **k** vertical tectonic fracture, medium-grained lithic–quartzose sandstone, Well T××–21, 2619.41~2619.59 m, drilling core

is 2.04 in the central Block B, the arithmetic mean pore throat diameter is only 1.02 μm at threshold entry pressure, 0.15 μm at 50% mercury saturation, the maximum mercury saturation ranges from 76 to 95%, and the arithmetic average ejection efficiency is only 36%, as shown in Fig. 5. The results of mercury injection measurement reveal small throat size, poor sorting, and weak connectivity of the pore throats in the strata of the central Block B. No porosity measurements using the mercury injection method has been carried out on sandstone reservoirs located in eastern Block B; therefore, there is no quantitative characterization of pore structure in the eastern Block B. Based on thin section observations, it is possible to say that pore types and widths from sandstones located within the middle and upper part of the stratigraphy in eastern Block B share similar characteristics than the pore throats from sandstones located in the central Block B. However, for the medium to coarse-grained lithic–quartzose sandstones located at the bottom part of the stratigraphy in the eastern Block B, the widths of lamellar throats among grains range from 1 to 8 μm, and the widths of microfracture throats crosscutting rigid grains and cements range from 3 to 18 μm mostly, as shown in Figs. 4d and 8d. Therefore, it is reasonable to suspect that the connectivity of reservoir pore throats in the eastern Block B should be better than that in the central Block B.

Table 2 Rock types (classified by grain sizes) of the Lower–Middle Jurassic reservoirs in Amu Darya right bank area

Section	Percentage of different rock types (%)			
	Siltstone	Fine-grained sandstone	Medium-grained sandstone	Coarse-grained sandstone
Lithofacies	Subaqueous natural levee, lakeshore sand bar, shallow-lake sand bank	Subaqueous distributary channel, lakeshore sand bar , shallow-lake sand bank	Subaqueous distributary channel, mouth bar	Subaqueous distributary channel, mouth bar
Upper section	39.51	55.19	5.30	0.00
Lower section	17.35	60.89	4.15	17.61
Whole strata	30.19	57.59	4.81	7.41

Table 3 Clastic constituents of the Lower–Middle Jurassic reservoirs in Amu Darya right bank area

Rock type	Number of samples	Percentage of framework grains(%)									Percentage of interstitial materials(%)				
		Quartz	Feldspar	Flaky minerals	Lithic fragments					Total amount of fragments	Matrix		Cement		
					Sedimentary lithic fragments			Metamorphic lithic fragments	Magmatic lithic fragments		Clay mineral	Kiesel	Carbonate	Kiesel	Authigenic clay mineral
					Quartzose fragments	Claystone fragments	Limestone fragments								
Lithic sandstones	6	28.00	10.42	3.15	6.46	19.54	3.98	6.82	0.96	37.76	9.80	0.67	8.86	0.13	1.21
Feldspathic–lithic sandstones	5	27.02	14.58	3.42	9.48	17.06	2.77	10.43	2.02	41.76	7.03	0.55	2.64	0.35	2.66
Lithic arkose	2	49.43	16.53	1.17	2.24	3.48	0.93	1.98	1.14	9.78	13.45	0.93	7.89	0.41	0.41
Lithic–quartzose sandstones	10	66.23	3.08	0.51	6.38	4.85	0.00	3.11	1.47	15.80	2.89	0.17	2.19	4.51	4.62

Table 4 Rock types (classified by lithologic composition) of the Lower–Middle Jurassic reservoirs in Amu Darya right bank area

Section/region		Percentage of different rock types (%)			
		Lithic sandstones	Feldspathic–lithic sandstones	Lithic arkose	Lithic–quartzose sandstones
Central Block B	B××–21	37.31	56.90	0.00	5.78
	Y××–23	72.53	21.98	5.49	0.00
Eastern Block B	T××–21	24.69	16.05	22.22	37.04
	G××–21	6.69	19.73	25.42	48.16
Upper section		42.93	31.09	16.28	9.70
Lower section		12.62	24.92	10.73	51.74
Total		31.72	28.81	14.23	25.24

Based on the analysis on pore structure above, large pore with fine throat and medium pore with microthroat are the typical two types of pore–throat combination of reservoir sandstones in the study area.

Drilling cores and FMI interpretations reveal that laminae fractures are the predominant type of fracture in the study area (Table 6). The average density of laminae fracture is 5.37 per meter in the study area, but it is much higher locally in the eastern Block B. For example, the density of laminae fracture increase to 40 per meter locally in drilling cores of Well G××–21 from 2890.99m to 2892.40 m, as shown in Fig. 4h. Stylolites infrequently occur in the study area and are fully filled by organic material fundamentally (Fig. 4g). Tectonic fractures develop poorly in the study area with the average density of 2.19 per meter. The dominated types of tectonic fractures are diagonal fractures in the central Block B, high-angle and vertical fractures in the eastern Block B (Fig. 4k, Table 6).

Parallel laminae ranging from 0.05 to 1.5 mm in thickness are observed occasionally in the reservoir sandstones. Laminae surfaces are relatively weak interfaces, easy to fracture by high pressure diagenetic fluid percolation or tectonic stress (Zhijun et al. 2003). Core observation shows that laminae fractures in the study area are generally horizontal or low-angled. Most laminae fractures in medium–coarse-grained sandstones are considered to be open underground. This assumption is based on (1) the presence of asphalt and oil trace on the fracture planes (Fig. 4i) and (2) the slight dissolution phenomenon along fractures (Fig. 4h). While laminae fractures in fine-grained sandstones and siltstones are supposed to be closed underground, and then are opened at shallow burial depth due to stress release, since no cementing material is observed in these laminae fractures and the width of fractures is generally less than 0 .3mm, some of these laminae fractures are even too short to crosscut the cores (Fig. 4j). The common width of tectonic fractures observed in cores ranges from 0.1 to 2 mm, and the trace length of high-angle and vertical tectonic fractures is mainly less than 0.3 m in the central Block B, but ranges from 0.1 to 1 .8 m in the eastern Block B (Fig. 4k). Most of the tectonic fractures are unfilled or partly filled by quartz or asphalt. Dissolution phenomenon along tectonic fractures is also observed occasionally (Fig. 4k).

According to 493 core porosity and permeability data, the average reservoir porosity is 7.53%, while the average reservoir permeability is 0.52 mD. Reservoir porosity values from the upper part of the stratigraphic interval range from 5.00 to 12.28% with an average value of 7.13%, while the reservoir permeability values range from 0.01 to 2935.11 mD with an average value of 0.25 mD. The porosity and permeability ranges of the lower part of the stratigraphy are 5.00–14.78%

Table 5 Pore types and pore diameter of the Lower–Middle Jurassic reservoirs in Amu Darya right bank area

Region	Well name	Number of samples	Percentage of different types of pore (%)				Main range of pore diameter (μm)			
			Primary pores	Secondary pores			Primary pores	Secondary pores		
				Intragranular dissolved pores	Intergranular dissolved pores	Intercrystal pores		Intragranular dissolved pores	Intergranular dissolved pores	Intercrystal pores
Central Block B	B××–21	6	0.46	46.25	41.72	11.57	30~60	60~200	40~90	< 15
	Y××–23	1	0.00	19.40	74.63	5.97	0.00	70~120	40~80	< 10
Eastern Block B	T××–21	1	0.00	25.00	75.00	0.00	0.00	20~60	30~300	0
	G××–21	12	3.32	16.23	74.57	5.88	60~100	50~150	60~280	< 20
Total		20	2.13	25.83	64.74	7.30	30~100	50~200	40~280	< 15

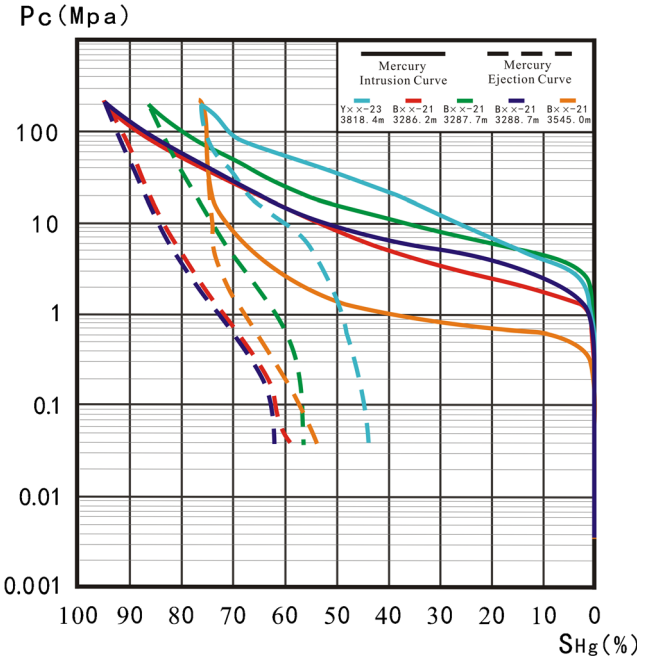

Fig. 5 Capillary pressure curves of the Lower–Middle Jurassic reservoirs in Amu Darya right bank area

and 0.07–7542.07 mD, and their respective average values are 7.68% and 0.69 mD. In comparison, reservoir characteristics are better for the lower part than for the upper part of the stratigraphy. Moreover, it appears the reservoir quality decreases from west to east within the area of interest. Indeed the average porosity of reservoirs is higher in Block A and central Block B, while the mean permeability is slightly higher in the eastern Block B (Table 7). The porosity and permeability ranges of the whole Lower–Middle Jurassic reservoirs in the study area are shown in Table 7 and Fig. 6.

The scatter plot in Fig. 7 shows that the relationship between permeability versus porosity of the cored Lower–Middle Jurassic reservoirs. In the upper section, permeability values generally do not increase along with porosity values, and even samples with porosity values higher than 10% are associated with low permeability values lower than 0.1 mD. This characteristic most likely indicates a poor interconnection between pores within the reservoir rocks due to narrow pore throats and limited number of effective fractures. In comparison, the permeability versus porosity relationship for the lower stratigraphic section is characteristic of higher quality reservoir facies most likely due to better connectivity within the sandstones. Combined with core observation, samples with high permeability (> 100 mD) are generally taken from cored intervals with tectonic fracture or laminae fracture. Porosity values of these samples are basically higher than the values from adjacent intervals without fractures. Consequently, it is obvious that fractures, although limited, take an important role in the reconstruction of both storage and connectivity capacity of reservoir rocks. In general, the Lower–Middle Jurassic reservoirs can be classified as pore-dominated sandstone reservoirs with limited fractures, characterized by very low porosity and permeability.

Table 7 Average porosity and permeability of the Lower–Middle Jurassic reservoirs Amu Darya right bank area

Region	Block A	Central Block B	Eastern Block B	Whole study area
Porosity	7.81	7.66	6.63	7.53
Permeability	0.40	0.60	0.69	0.52

Main controlling factors on reservoir characteristics

Sedimentation

Clastic constituents

Reservoir compaction and diagenetic processes are strongly influenced by the mineralogical composition of the reservoir

Table 6 Fracture development of the Lower–Middle Jurassic reservoirs in Amu Darya right bank area

Region	Well name	Interval	Thickness (m)	Fracture density (number of fractures per meter)						
				Laminae fracture	Stylolite	Tectonic fracture				Total
						Horizontal (< 10°)	Low-angle (10~40°)	High-angle (40~70°)	Vertical (> 70°)	
Central Block B	B××–21	3278.80~3282.00	3.2	4.38	0.31	0.00	0.31	0.00	0.00	5.00
		3284.00~3294.30	10.3	3.69	0.00	0.29	0.68	0.19	0.00	4.85
		3542.40~3545.80	3.4	6.47	0.59	0.29	0.59	0.29	0.00	8.23
	Y××–23	3811.40~3816.80	5.4	3.33	0.00	0.19	0.19	0.93	0.00	4.64
Eastern Block B	T××–21	2617.20~2620.10	2.9	4.48	0.34	0	0.69	2.07	1.72	9.30
	G××–21	2244.10~2245.40	1.3	0.00	3.08	1.54	0.77	0.77	2.31	8.47
		2887.00~2894.76	7.76	10.18	1.93	0.90	1.03	1.16	0.90	16.10
Average			4.89	5.37	0.67	0.41	0.64	0.70	0.44	8.23

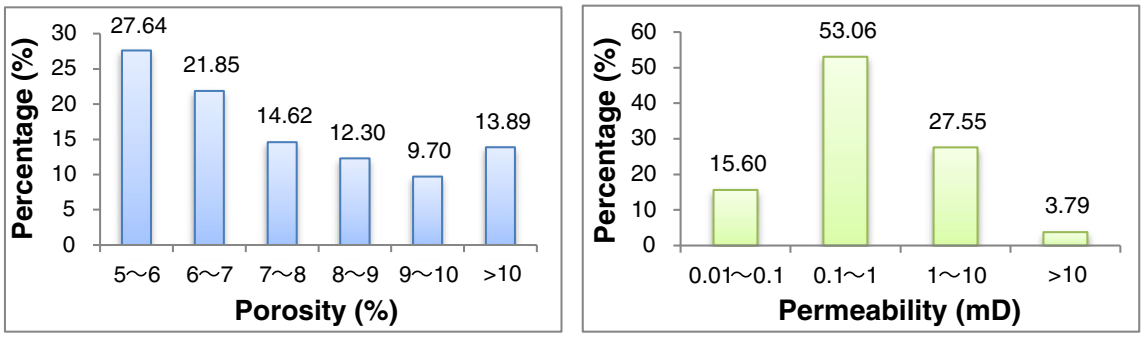

Fig. 6 Histograms of porosity and permeability distributions of the Lower–Middle Jurassic reservoirs in Amu Darya right bank area

rocks. It is commonly accepted that compressive strength of rigid grain is higher than the compressive strength of ductile grains. Thin sections and SEM photomicrographs show that, due to high overburden stress, brittle fractures are observed occasionally in quartz grains and feldspar grains (Fig. 8d, e), while plastic deformation is commonly observed in ductile lithic fragments and flaky minerals, such as claystone fragments, phyllite fragments, and white mica (Fig. 8a, b). In comparison to lithic–quartzose sandstones, the primary porosity is lower in lithic sandstones and feldspathic–lithic sandstones. This is because the latter type of sandstones are composed largely by both ductile grains and rigid grains, with ductile grains strongly squeezed into irregular shape against rigid grains and intruded into spore spaces as a as pseudomatrix (Fig. 8a, b). Furthermore, thin sections and core porosity data indicate that secondary dissolution porosity is more common in lithic–quartzose sandstones than in lithic sandstones. In G××–21, for example, shows an average dissolution porosity in feldspathic–lithic sandstones and lithic sandstones is of 1.48% and 1.96% for the stratigraphy, but the values range between 4.71% and 7.05% in lithic arkose and lithic–quartzose sandstones (Figs. 4d, 8d). We suggest that the differences of dissolution porosity among different rock types could be explained by the fact that the migration of diagenetic fluid was blocked dramatically in ductile grain-dominated sandstones, since the total volume of rocks together with

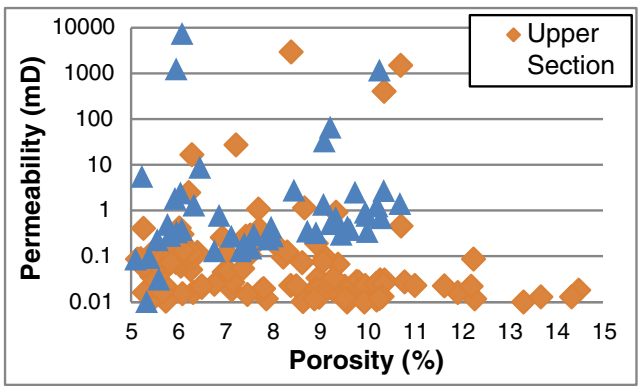

Fig. 7 Scatter plot of core permeability versus core porosity of the Middle–Lower Jurassic in Amu Darya right bank area

primary pores were reduced at a faster rate and more seriously by both compaction and calcite cementation processes during the early diagenetic stage and fluid pathways were strongly reduced in size and numbers. As shown in Table 4, lithic sandstones and feldspar–lithic sandstones represent very high proportions in the central Block B (94%) and the upper part of the stratigraphy (74%), while these proportions decrease to 34% in the eastern Block B and 38% within the lower part of the stratigraphy. Thus, it is reasonable to conclude that the compressive strength of reservoir rocks in the central area and upper part of the stratigraphy should be lower than the compressive strength of reservoirs located in the eastern area and lower part of the stratigraphy.

In addition, the size of framework grains is also an important component to look at with regard to pore space characterization in reservoir rocks. According to the experimental burial compaction of sandstone reservoirs done by Zhiyong G in 2013, the surface area to volume ratio is high on grains with small-diameter grains, thus it is more difficult for grains to slide or deform under overburden stress. This means that only a small amount of lithostatic pressure is accommodated by framework grains. Therefore, the porosity among fine-sized grains sandstones accommodates most of the lithostatic pressure and consequently decreases seriously. On the contrary, for sandstones composed predominantly of coarse-sized grains, their primary porosity and pore throats can be better preserved during the early diagenetic stage because framework grains accommodate most of the overburden stress, as evidenced by the microcracks on framework grains (Zhiyong et al. 2013). Moreover, primary pore spaces and microcracks on grains provide valid pathways for diagenetic fluids, thus dissolution is successively distinguished on reservoir sandstones with different grain size. Consequently, under the same diagenetic conditions, reservoir pore spaces of coarse–medium-grained sandstones should be better than that of fine grained sandstones and siltstones consist of the same constitutes. The result of analysis on core porosity of different grain size sandstones in the study area is consistent with the above conclusion. Figure 9 shows the positive relationship between core porosity of reservoirs and the grain sizes of feldspathic–lithic sandstones and lithic sandstones in the central Block B

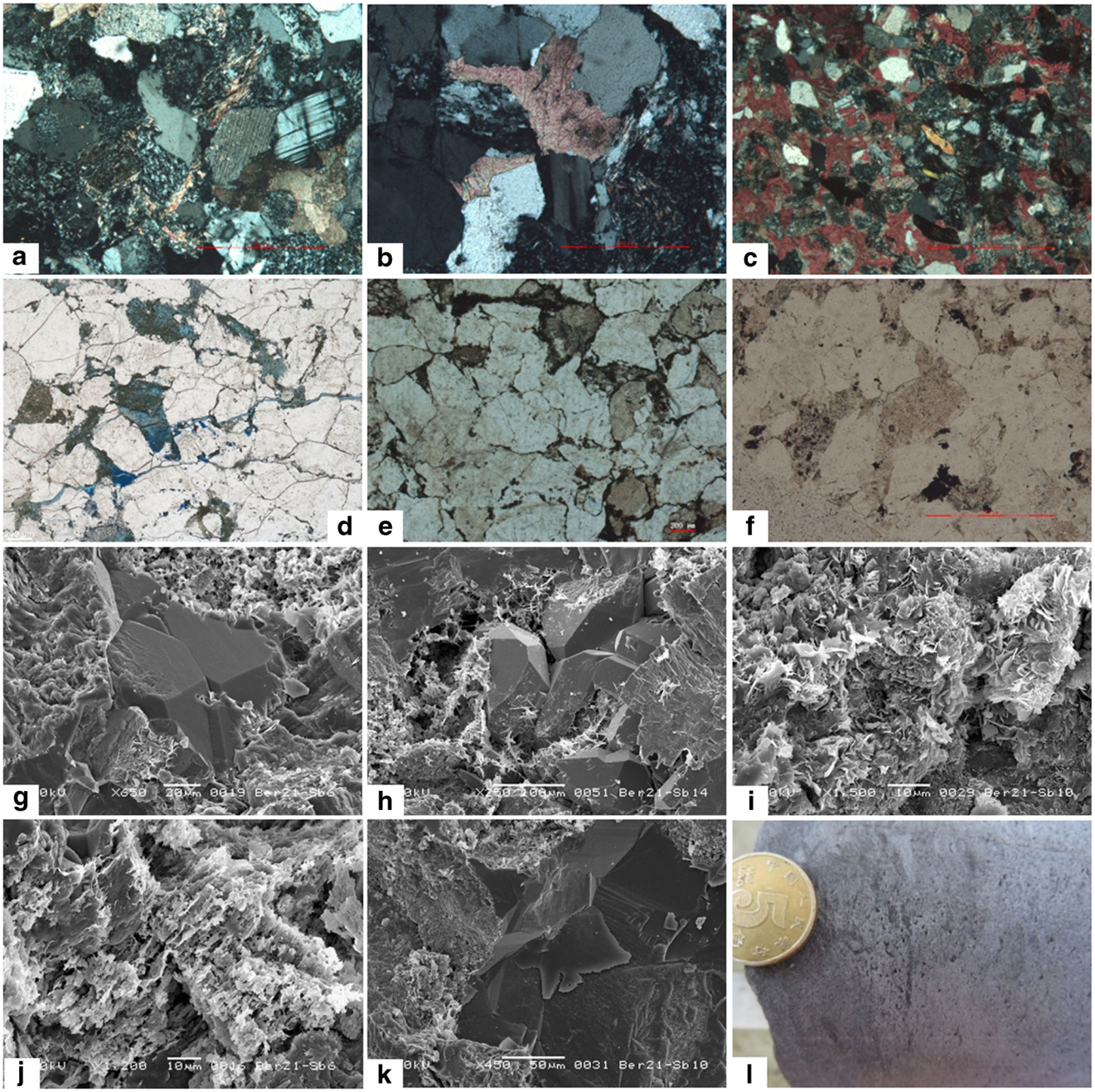

Fig. 8 Diagenesis of the Lower–Middle Jurassic reservoirs in Amu Darya right bank area. **a** Compaction and quartz overgrowths, medium-grained feldspathic–lithic, Well B××–21, 3284.10 m, scale bar represents 500 μm, crossed nicols; **b** compaction, cataclasis, and ferroan dolomite cementation, medium-grained lithic–quartzose sandstone, Well B××–21, 3542.95 m, scale bar represents 500 μm, crossed nicols; **c** calcite cementation, fine-grained lithic sandstone, Well Y××–23, 3812.80 m, scale bar represents 500 μm, crossed nicols; **d** quartz overgrowths, cataclasis, dissolution, and kaolinite cementation, coarse-grained lithic–quartzose sandstone, Well G××–21, 2890.43 m, scale bar represents 200 μm, plain light; **e** pressure solution, compaction, siderite cementation, quartz overgrowths, coarse-grained lithic–quartzose sandstone, Well G××–21, 2887.50 m, scale bar represents 200 μm, plain light; **f** kaolinite is the product of feldspars alteration, medium-grained feldspathic–lithic, Well B××–21, 3546.00 m, scale bar represents 500 μm, plain light; **g** quartz overgrowths, medium-grained lithic–quartzose sandstone, Well B××–21, 3284.10 m, scale bar represents 20 μm, scanning electron microscope; **h** quartz overgrowths, fine-grained lithic–quartzose sandstone, Well B××–21, 3545.00 m, scale bar represents 100 μm, scanning electron microscope; **i** honeycomb illite cements and foliated chlorite cements, fine-grained feldspathic–lithic sandstone, Well B××–21, 3292.7 m, scale bar represents 10 μm, scanning electron microscope; **j** dissolution, medium-grained feldspathic–lithic sandstone, Well B××–21, 3284.10 m, scale bar represents 10 μm, scanning electron microscope; **k** dissolution, quartz overgrowths, Well B××–21, 3292.70 m, scale bar represents 50 μm, scanning electron microscope; **l** Dissolution, fine-grained feldspathic–lithic sandstone, Well G××–21, 2255.53–2255.69 m, drilling core

(Well B××–21 and Well Y××–23). The average porosity of medium-grained and fine-grained feldspathic–lithic sandstones is 9.14% and 8.51%, respectively, while the mean porosity of feldspathic–lithic siltstones is only 6.87% (Fig. 9). As mentioned above, more than 87% of reservoir rocks are fine-grained sandstones and siltstones, while medium–coarse-grained sandstones account for less than 13%. Therefore, the fine and very fine clastic constituents of reservoir rocks are generally detrimental for reservoir quality in the study area.

Lithofacies

Study shows that sandstones of the Lower–Middle Jurassic strata are associated with different lithofacies characterized by a broad spectrum of lithology with various petrophysical properties.

Coarse-grained and medium-grained sandstones are present predominantly in subaqueous distributary channel and mouth bar lithofacies in the study area. Fine-grained sandstones represent a large proportion of reservoir rocks in subaqueous distributary channels and lakeshore sand bars, while siltstones are mostly present in shallow-lake sand banks. Thus, subaqueous distributary channels and mouth bars are the best reservoir lithofacies for reservoir development in the study area, with an average porosity of 7.92% and 7.74%, mean permeability of 0.66 mD and 0.63 mD respectively. Lakeshore sand bars and shallow-lake sand banks come the third and fourth place (Fig. 10). Based on the common occurrence of subaqueous distributary channels and mouth bars lithofacies within the Lower Jurassic interval, and the common occurrence of shallow lacustrine sand bank lithofacies within the Middle Jurassic strata, we suggest that this difference of depositional environment constitute a reasonable explanation for the difference of reservoir quality between the lower and upper part of the stratigraphic column.

Diagenesis

Various types of diagenetic processes also have great impaction on evolution of the Lower–Middle Jurassic reservoirs, according to the microscopic observations. Among the different diagenetic processes, compaction, cementation, and dissolution seem to have modify the initial rock property the most.

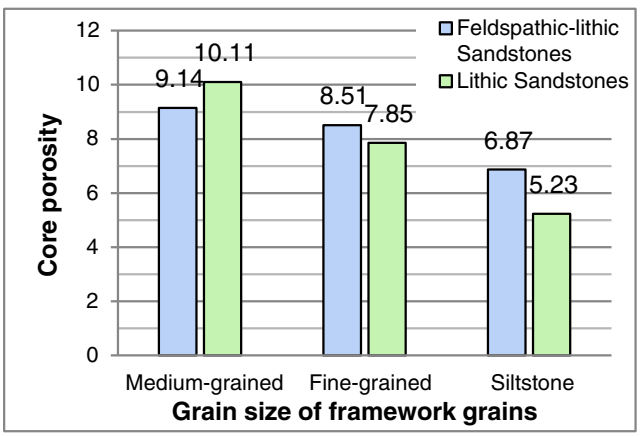

Fig. 9 Porosity of different grain size sandstones in the central B Block of Amu Darya right bank area

Compaction

As mentioned above, compressive strength of reservoir rocks in the central Block B is generally low, since ductile grains account for a large proportion of the clastic constituents (Tables 3 and 4). In addition to constituents, the degree of compaction also largely depends on burial depth, paleogeothermal temperature, and subsidence style (Jianfeng and Guohua 1998; Jianfeng et al. 2006). Burial history study (Qiang et al. 2014) reveals that the maximum burial depths of the bottom of the strata gradually increase from west to east in the study area, and are more than 4000 m in the central Block B, up to 6000 m in the eastern Block B (Table 8). Previous study shows that, during the Neogene, the maximum paleogeothermal temperature associated with the Callovian to Oxfordian carbonates strata was approximately 140°C in Block A (Yan et al. 2011). Therefore, during the Neogene, the maximum paleogeothermal temperature of the Lower–Middle Jurassic strata in Block A should be higher than 140°C. Fluid inclusion homogenization temperature measured on primary inclusions within quartz overgrowths taken from the bottom of the Lower–Middle Jurassic strata of Well T××–21 indicates that during the Neogene, the average paleogeothermal temperature in the eastern Block B is 152 °C. Besides, earlier researches on tectonic evolution illustrate that the study area had a continuously high subsidence rate during Jurassic and the Early–Middle Cretaceous Periods (about 27–32 m/Ma), then kept the deep burial depth during Paleogene, and rapidly uplifted (about 17.1–137.34 m/Ma) from Neogene Period to present days (Yudan and Chunguang 2014). According to Jianfeng Shou (Jianfeng and Guohua 1998), the subsidence process in the study area is the worst subsidence type for porosity protection because of the deep burial depth, high paleogeothermal temperature, and high subsidence rate during the early diagenetic stage.

High subsidence rate during the early diagenetic stage (about 40–43 m/Ma), deep burial depth and its resulting high overburden stresses, high paleogeothermal temperature (> 140 °C), and together with the low compressive strength of reservoir rocks most likely led to strong mechanical compaction and slight pressure solution in Block A and the central Block B. Figure 8a and b show the tight mineral organization, the common deformation of ductile grains, the brittle fractures of rigid grains, and the concave–convex sutured contacts of framework grains from samples located in the central Block B.

In spite of the relatively high percent of lithic–quartzose sandstones in reservoir rocks (Table 4), the combination of high paleogeothermal temperature (152 °C), high subsidence

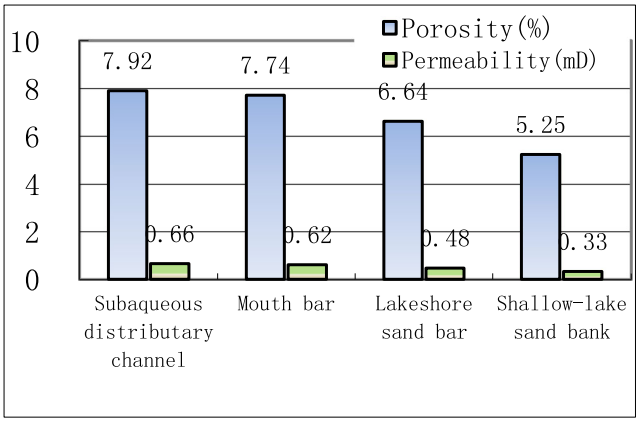

Fig. 10 Porosity and permeability of different kinds of lithofacies of the Lower–Middle Jurassic in Amu Darya right bank area

rate during the early diagenetic stage, and the deep maximum burial depth (> 5350 m) in the eastern Block B (Fig. 11) also resulted in significant destruction of primary porosity. Thin sections from both G××–21 and T××–21 show that the framework grains commonly become reoriented along the longer axes and generally in long linear contacts (Figs. 4d, 8d). Non-directional intragranular cracks are observed on small portion of framework grains (Fig. 8d, e). Pressure solution is occasionally observed in eastern Block B too, especially in lithic–quartzose sandstones. Figure 8d and e shows interlocking phenomenon and concave–convex to sutured contacts between quartz grains. Due to the high pressure among grains, some quartz mineral dissolved in the presence of pore water, then was moved and precipitated on free surface of the grains, therefore, provided silica for the quartz overgrowth in the latter digenetic stage (Gary 2014; Xinghe 2010).

Cementation

Cementation is another important diagenetic process which often has negative effects on reservoir properties, since cements lithify sedimentary deposits and fill up pore spaces. There are three major types of cementation present in the Lower–Middle Jurassic sandstone reservoirs in the study area, which are carbonate cementation, quartz cementation, and clay mineral authigenesis.

(1) Carbonate cementation

Carbonate cementation is common in the Lower–Middle Jurassic reservoir rocks. The most usual carbonate cements are microcrystalline to fine-crystalline calcite (according to National Standard of the People's Republic of China GB/T 17412.2-1998), precipitating in primary intergranular pores with crystal size varying from 0.03 to 0.1 mm (Fig. 8c). Figure 8c shows that calcite cements in the study area precipitated during the eogenetic stage, before effective compaction. This interpretation is based on the cementation style of calcite cements which is either basal cementation or porous cementation. The relative abundance of calcite cements, recognized in thin sections, decreases seriously from the top to the bottom of the stratigraphic column. In Well B××–21, for example, the average proportion of calcite cements in sandstones is 5.8% at the top of the upper section, but decreases down to 2.0% in the middle part of the stratigraphic column. In combination with the sedimentary study, it is reasonable to conclude that the eogenetic calcite cementation of reservoir sandstones is closely related to the marine–continental transitional environment, and the calcite cements in the top of the strata is supposed to originate from limestone lithic fragments and the aragonitic shelly material deposited along with the sand. Although, eogenetic calcite cementation largely enhanced the compressive strength of sediments during the early diagenetic stage and inhibited compaction dramatically, primary pores are commonly filled and destroyed by calcite cements (Fig. 8c). Therefore, calcite cementation is detrimental for the reservoir quality in the study area.

Fine-crystalline to medium-crystalline ferroan dolomite cementation occur occasionally in lithic sandstones and feldspathic–lithic sandstones in proportion less than 5% (Fig. 8a) of the whole rock volume, but rarely occur in lithic–quartzose sandstones (Fig. 8b). Observation of thin sections reveals that, the appearance of ferroan dolomite cements occurred after the effective compaction and before the late uplift event, based on the fact that framework grains cemented by ferroan dolomite are still well compacted (Fig. 8a, b) and microfractures generated by tectonic movement during Neogene and Quaternary Periods crosscut both framework grains and ferroan dolomite cements, as shown in Fig. 8b. Consequently, ferroan

Table 8 The maximum paleoburial depths of the bottom of Lower–Middle Jurassic strata in the Amu Darya right bank area

Region	Western Block B	Block A	Central Block B	Eastern Block B		
Well Name	Nf××–21	S××53–1	B××–21	A××–22	T××–21	Outcrop
The maximum paleoburial depths (m)	3200	3500	4200	5350	5960	> 6100

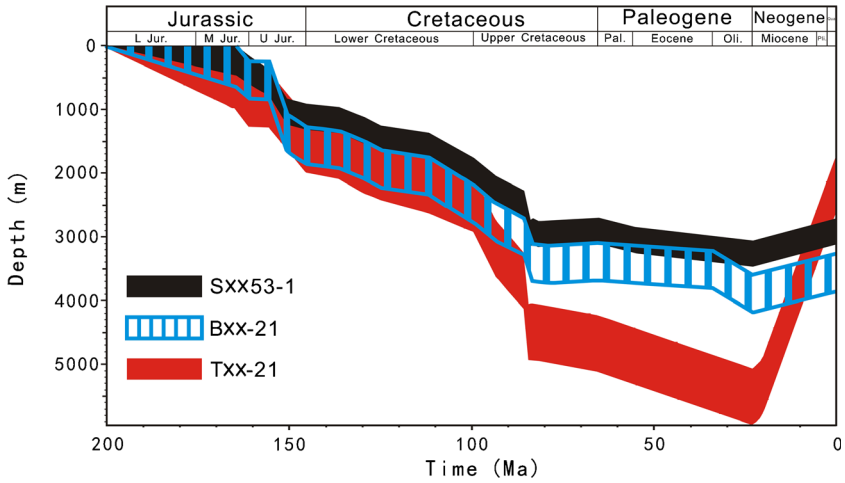

Fig. 11 Burial history paths of the Lower–Middle Jurassic in Amu Darya right bank area

dolomite cements cannot increase the compressive strength of reservoir sandstones, and completely fill up the remaining intergranular pores. Furthermore, no dissolution phenomenon of ferroan dolomite was observed in the study area based on the available core data (Fig. 8a, b). This indicates that the destruction of ferroan dolomite cementation on reservoir sandstones is effective and irreversible.

Siderite cementation is rarely observed in lithic–quartzose sandstones with the maximum proportion less than 4%. Consisting mostly of micrite siderite, siderite cements precipitate on the surface of grains and envelop grains as thin films with the thickness ranging from 0.005 to 0.02 mm (Fig. 8e). It is worth noting that siderite thin films do not precipitate on the surface of host quartz grains, but on the surface of overgrowths of quartz. Grains cemented by siderite are also in long linear contacts to concave–convex contacts (Fig. 8e). Therefore, siderite cementation of the Lower–middle Jurassic strata is considered to take place after both effective compaction and quartz cementation, and have no positive effects on the preservation of pore space in the study area.

(2) Quartz overgrowths

Authigenic quartz overgrowths are intensive and commonly observed in all kinds of sandstones in the study area (Fig. 8a–h), but it is weak and uncommon at the top of the stratigraphic column where calcite cementation is dominant and compaction is weakly expressed, because according to Gary N, the diffusion of host quartz grains in pressure solution is one of the main source of silica which is indispensable to quartz overgrowths (Gary 2014). Thin sections show that the original subrounded quartz grains are widened and sharpened by secondary growths, some at isolated points but most around the whole surface. The widths of overgrowth rims are mainly ranging from 0.03 to 0.1 mm, the volume of overgrowths are commonly equal to a quarter to a half of the host grain volume (Fig. 8a–f). SEM photomicrographs reveal that secondary quartz crystals in the study area are hexagonal pyramid shaped, clean, and intact, with clear crystal faces and crystal edges (Fig. 8g, h). Lengths of secondary quartz crystals usually range from 0.05 to 0.1 mm, and the diameter of crystals are generally less than 0.05 mm. Figure 8g and h present the connection and mosaic structure among adjacent authigenic quartz crystals. As secondary quartz growing out into pore spaces, further compaction were inhibited to some extent, but previous remaining intergranular pores are largely occupied by quartz overgrowths (Fig. 8g) or replaced by intercrystal pores with diameter less than 0.02 mm (Fig. 8h), and only small amount of remaining intergranular pores among rigid grains can be preserved, mostly in lithic–quartzose sandstones. Therefore, it is concluded that quartz overgrowths reduced intergranular porosity further and are detrimental for the reservoir quality in the study area.

(3) Authigenic clay mineral cementation

Based on thin sections and SEM photographs, authigenic clay mineral cements of the Lower–Middle Jurassic reservoir sandstones include kaolinites, illites, chlorites, and small amounts of mixed–layer illite/montmorillonites. Kaolinite cements account for about 2% on average in the Lower–Middle Jurassic strata and are more commonly observed in lithic–quartzose sandstones. Al^{3+} and SiO_3^{2-} ions are released from the reaction of alkali feldspars and acidic fluids, and when pore water is saturated with Al^{3+} and SiO_3^{2-}, authigenic kaolinites precipitate (Xin et al. 2016). Under electron microscope, kaolinite crystals are pseudohexagonal, in shape of sheet and commonly highly automorphic (Fig. 4e, f). Some authigenic kaolinites occupy the intragranular dissolved pore spaces of feldspar grains, as shown in Fig. 8f. Feldspar grain in the center of Fig. 8f is almost entirely replaced by authigenic kaolinites, and only the residual rim of feldspar grain is observed. Authigenic kaolinites precipitated on the surface of framework grains or grow out into intergranular pores (Figs.

Table 9 Porosity and permeability of the Lower–Middle Jurassic reservoirs in the Amu Darya right bank area

Region	Block A	Central Block B	Eastern Block B
Matrix porosity (%)	7.76	7.50	6.37
Matrix permeability (mD)	0.39	0.45	0.43
Final porosity (%)	7.81	7.66	6.63
Final permeability (mD)	0.40	0.60	0.69

4f and 8d, f). It is worth noting that authigenic kaolinites precipitate on the surface of authigenic quartz, as shown in Fig. 4f. This means that kaolinite cements mostly precipitated after quartz overgrowths in the study area. Besides, the edges of some kaolinite crystals become thin and fibrous, as shown in Fig. 4e and the right side of Fig. 4f. According to previous researches, this phenomenon is the evidence of illitization of kaolinite which generally take place when the temperature is higher than 120–140 °C and burial depths are more than 3600 m (Sijing et al. 2009; Wanbin et al. 2011). Kaolinite precipitation has constructive effects on reservoir characteristics. Thin sections and SEM photomicrographs reveal that the precipitation of authigenic kaolinites is always associated with the dissolution of feldspars, and authigenic kaolinites can be viewed as the products of feldspar alteration. Thus, the appearance of authigenic kaolinites signifies feldspar dissolution which is beneficial for reservoir evolution (Fig. 4e, f).

Authigenic illite cements account for only 0.5% of rock samples on average in the Lower–Middle Jurassic strata. Three shapes of authigenic illites are observed in the study area, and the genesis of each shape of illites is different. Honeycomb structure is the most common structure of illites. Illites with honeycomb structure are transformed from montmorillonites, since mixed layer illite/montmorillonites are occasionally identified together with honeycomb illites by SEM and EDS. Filamentous illites usually precipitate along the cleavages on the surface of dissolved feldspars (Fig. 8j), or deposit in the intragranular dissolved pores of feldspars. Filamentous illites are considered to be the products of potassic feldspar alteration (e.g., Sijing et al. 2009; Wanbin et al. 2011). As mentioned above, illitization of kaolinites is observed occasionally in the study area. Illite crystals transformed from kaolinites are flake-like in whole, but the edges of crystals are usually fibrous (Fig. 4e, f). Illites precipitation has double effects on reservoir quality in the study area. Honeycomb and filamentous illites grow out into pores from the surface of framework grains and crosscut the original pores into smaller and more curved spaces; therefore, fluid pathways become narrower and curvier. Permeability of reservoir sandstones is reduced by authigenic illite cementation as a consequence. However, previous studies have shown that both transformation of montmorillonites into illites and illitization of kaolinites in a sealed environment definitely lead to the dissolution of potassic feldspar, and secondary dissolved pores are produced in the processes (Sijing et al. 2009; Wanbin et al. 2011). Furthermore, Hurst and Nadeau presented that the average intercrystal porosity of authigenic illites is 63%, and the average intercrystal porosity of authigenic kaolinites is only 43% (Andrew and Paul 1995); thus, illitization of kaolinites is beneficial for the increase of intercrystal porosity.

Similar to the proportion of authigenic illites, the proportion of authigenic chlorites in the study area is low and less than 0.5% of rock samples. Chlorite crystals in the study area are leaf-like or acicular, occupying intergranular pores together with illite crystals (Fig. 8i), or sparsely precipitating on the grain surface as grain coatings according to thin sections and SEM photomicrographs. It is commonly admitted that chlorite coatings growing at an early stage can reduce the extent of compaction and delay quartz overgrowths by reducing the available quartz surface (SN Ehrenberg 1993; Quanli et al. 2012). However, chlorite coatings are observed very rarely in the study area, the preservation of porosity thereby is insignificant. In contrast, authigenic chlorite crystals that precipitated during the mesogenetic stage grow into the adjacent pore spaces, and occupy pore volume just like other clay mineral cements. Overall, chlorite cementation has both a positive and a negative effect on reservoir physical properties, but because of the low contents, the influence of authigenic chlorites on reservoir evolution is negligible.

Dissolution

Dissolution is relatively common in the study area. According to Table 5 and the average porosity in the study area, it is calculated that the mean dissolution porosity of sandstone reservoirs is 6.82%, and that is 90.57% of the total porosity. Dissolution phenomenon is occasionally observed in drilling cores. For example, acicular-dissolved pores with diameter ranging from 0.3 to 0 .5 mm distribute on the surface of feldspathic–lithic sandstone cores of Well Gok–21from 2255.53m to 2255.69m (Fig. 8l). Under electron microscope, dissolution phenomenon is more common. Thin sections and SEM photomicrographs reveal that dissolution usually occurs in lithic and feldspar grains; thus, both intragranular and intergranular dissolved pores are more likely to develop around these two kinds of grains (Figs. 4c, d and 8d). Figure 8j shows the strong dissolution along cleavages of one feldspar grain, and the surface of dissolved grain is fenester and porous. Dissolution of quartz framework grains is less common in the study area due to the higher stability of quartz mineral. It is revealed in Fig. 8d that the brim of a few quartz framework grains is embayed and irregular as a result of slight dissolution. Besides the dissolution of framework grains, cement dissolution is also observed. In Fig. 8k, the surface of authigenic quartz crystal is partly dissolved and small amount of

authigenic illite precipitate on it. However, there is no dissolution of carbonate cements observed in the study area according to the existing core data.

Formation water and organic acids originated from the maturation of organic matter are considered to be the dissolution fluids in the study area. As mentioned above, primary pores of lithic sandstones and feldspar–lithic sandstones were diminished more quickly and strongly by compaction during the early diagenetic stage, since contents of ductile grains which have low compressive strengths account for about 34% by volume (Table 3). As a consequence, migration of dissolution fluids were blocked dramatically in the early diagenetic stage and dissolution phenomenon is rare in lithic sandstones and feldspar–lithic sandstones (Fig. 8a, c). On the contrary, dissolution phenomenon is more frequently observed in lithic–arkose and lithic–quartzose sandstones, as a result of the relatively unrestricted flowing of dissolution fluids in the early diagenetic stage. Tectonic fractures and laminae fractures can also be the migration pathway of dissolution fluids. Core observations show that dissolved pores and holes often develop near fractures on drilling cores. For example, vertical tectonic fracture with the length of 3.32 m crosscuts drilling cores of Well Gok–21from 2253.00–2256.67 m, and acicular-dissolved pores distribute more densely in this cored interval than in others. Figure 8l shows one dense distribution area of acicular-dissolved pores in this interval. Besides, some dissolution phenomenon is observed along coring fractures. In Fig. 4h, laminae fractures are dissolved and slightly enlarged; therefore, the width of fractures is irregular.

Ions such as Na^+, K^+, Ca^{2+}, Al^{3+}, and Fe^{2+} are released during the dissolution process. Sandstone reservoirs of the Lower–Middle Jurassic strata are relatively isolated since they are enclosed within thick hydrocarbon source rocks; therefore, most of the ions released cannot flow away but stay in situ or nearby, and finally precipitate as authigenic minerals such as kaolinites and illite. Although the precipitation of authigenic minerals block up residual pores and throats, and reduce the porosity and permeability to some extents, most of the intragranular and intergranular pore spaces generated from dissolution are preserved and become the predominant pore spaces in the study area (Figs. 4c, d and 8d). In general, dissolution is the most beneficial diagenetic processes for the reservoir characteristics in the study area.

Tectonic movements

Structural evolution researches reveal that Amu Darya right bank area subsided steadily from Late Jurassic to Paleogene Period after the deposition of Lower–Middle Jurassic clastic strata, and only two small-scale tectonic movements took place during that time. Those two tectonic movements caused the deformation of Kimmeridge–Tithonian gypsum and salt beds of the Upper Jurassic strata and due to the plasticity of gypsum and salt beds, most of structural faults do not extend into the Lower–Middle Jurassic strata (Jianliang et al. 2010). The third tectonic movement which happened in Neogene and Quaternary Periods is the most significant tectonic movement in Amu Darya Basin. It was resulted from the collision of Indian, Arab, and Eurasian plates, and caused intensive uplift and deformation in Gissar region which is located in the eastern Block B (Shikuo et al. 2013). The uplift of Gissar Mountain made strong lateral extrusion from southeast to northwest across the study area. Acoustic emission examination shows that average paleotectonic stress of the Callovian–Oxfordian carbonate rocks in Neogene Period decrease from east to west obviously: average paleotectonic stress is 13.08 Mpa in Well A××–22 which located in the eastern Block B, while decreased to 6.74 Mpa in Well C××–21 in the central area, and is only 3.47 Mpa in Well S××45–1 situated in Block A. Intensive compressional stress from the southeast caused strong tectonic deformation to the whole Jurassic system. Seismic cross-sections reveal plastic deformation, small-scale compressional faults, and large-scale strike–slip faults in the Kimmeridge–Tithonian gypsum and salt beds, as well as the remarkable thrust faults with strike mainly in northeast–southwest direction in the Callovian–Oxfordian strata (Henian et al. 2013). Paleotectonic stress and tectonic deformation of the Lower–Middle Jurassic strata are slightly weaker than that of the upper formations. The average paleotectonic stress of the Lower–Middle Jurassic sandstones in Neogene Period is 2.22 MPa in Well B××–21, and is 4.10 MPa in Well Y××–23 which is located 22.96 km east from Well B××–21. Northeast–southwest trending thrust faults caused by compressional stress develop in the eastern and central Block B, and the scale of faults decreased from east to west as the tectonic stress weakened (Fig. 2). In the western study area, contemporaneous normal faults with strike in northwest–southeast direction were partly transformed into strike–slip faults by the Neogene–Quaternary tectonic movements, since the compressional stress from southeast was basically parallel with the strike of faults (Shikuo et al. 2013).

The uplift of Gissar Mountain in the Neogene–Quaternary Periods certainly generated tectonic fractures of the Lower–Middle Jurassic strata as well. For example, two micro fractures with the length more than 1.30 mm are observed in the middle of Fig. 8d. They penetrate quartz framework grains, quartz overgrowths, and even authigenic kaolinites (Fig. 8d). In Fig. 8b, one microfracture crosscut both quartz grain and ferroan dolomite cements. Therefore, those micro fractures are considered to be generated by the late tectonic movements rather than the early mechanical compaction, since the generation of fractures took place after quartz cementation, kaolinite cementation and ferroan dolomite cementation. As mentioned above, the average fluid–inclusion homogenization temperature of fracture filling (Quartz) at 2619.41m of Well Tag–21 is 152 °C. The burial depth is calculated to be about 3900 m

when the fracture was filled, based on a mean surface temperature of 25 °C and a paleogeothermal gradient of 30–35 °C/km in Amu Darya Basin (Yan 2013). According to the Burial history path of Well Tag–21 in Fig. 11, the burial depth was 3900 m in both the middle stage of Cretaceous Period and the late stage of Miocene Epoch. Since there was no tectonic movement happening in the middle Cretaceous Period, it is reasonable to conclude that the tectonic fracture was generated slightly before the Late Miocene by the Neogene–Quaternary tectonic movements. It is worth noting that the Neogene–Quaternary tectonic movements also resulted in the generation of laminae fractures in the study area. Drilling core observation shows the negative relationship between laminae fractures and tectonic fractures in the study area (Table 6). For example, 40 laminae fractures developed intensively at the bottom of the Lower–Middle Jurassic strata of Well Gok–21 from 2890.99 to 2892.40 m, while only one low-angle tectonic fracture with the length of 0.12 m developed within that cored interval. Instead, seven tectonic fractures, including three vertical fractures with the length ranging from 0.27 to 0.81 m developed in the cored interval of Well Gok–21 from 2244.10 to 2245.40 m, but no laminae fracture were observed with in that interval. Based on the previous study about laminae fractures, it is concluded that parts of the tectonic stress in the study area were released through the laminae surface, which are the weak interfaces of the strata, thus parallel laminae fractures develop locally. As a result of the stress relaxation, the development of tectonic fractures is restricted and poorer in those laminae fracture developed area.

The impact of tectonic movements on the Lower–Middle Jurassic sandstone reservoir is of paramount importance. As mentioned above, studies on clastic constituents of reservoir rocks reveal that the compressive strength of reservoir sandstones is higher in the eastern Block B. However, the paleoburial depths of the strata is up to 5300 m in the eastern Block B after the continuous subsidence from Jurassic to Paleogene Periods and that is 1100 to 2500 m deeper than that in Block A and the central Block B (Table 8, Fig. 11). Undoubtedly, the overburden stress of reservoir rocks in the eastern Block B should be stronger during Jurassic to Paleogene Periods. Moreover, the uplift of Gissar Mountain in the Neogene–Quaternary Periods made strong lateral extrusion from the southeast, thus the lateral compressional stress in the eastern Block B was more intense, which can be proved by the sharp upraise, more thrust faults and fractures in the area (Fig. 2, Table 6). The stronger overburden stress and higher lateral compressional stress jointly made the poorer matrix pore development in the eastern Block B, in spite of the higher compressive strength of reservoir rocks. Statistics show that the matrix porosity and permeability of reservoirs are 7.76% and 0.39 mD in the western area, 7.50% and 0.45 mD in the central Block B, but only 6.37% and 0.43 mD in the eastern Block B (Table 9). However, thrust faults and fractures generated by tectonic movements improved the physical properties, especially the permeability of reservoir rocks in the study area. Statistics of 493 core porosity and permeability data from all the 4 cored wells show that, the average porosity and permeability is 7.21% and 0.53 mD respectively in fracture developed cored intervals, but only 6.83% and 0.13 mD in cored intervals without any fracture. Figure 2 and Table 6 exhibit that faults and fractures developed better in the eastern Block B; therefore, although the matrix porosity and permeability in the eastern Block B are lower than those in the western area, the mean permeability of reservoirs in the eastern Block B, which is 0.69 mD, is obviously higher than the mean permeability in the middle and the western area (Table 9). Meanwhile, as stated above, fractures can also be the migration pathways for dissolution fluids, so they are beneficial to the dissolution of reservoir sandstones. In general, tectonic movements have double impacts on the Lower–Middle Jurassic sandstone reservoirs. Reservoir matrix porosity and permeability become worse due to the lateral compressional stress of tectonic movements, but the resultant fractures provide valid percolation paths in reservoir rocks, as a consequence, have positive effects to reservoir evolution.

Conclusions

1) Fine-grained sandstones and siltstones are the main types of reservoir sandstones of the Lower–Middle Jurassic strata, while coarse- and medium-grained sandstones are present in small amounts. Lithic and feldspar–lithic sandstones with low compressive strength account for high proportions in the central Block B and the upper section of the strata, while lithic–quartzose sandstones are the main types of reservoir rocks in the eastern Block B and the lower section of the strata. Generally, reservoir sandstones are characterized by moderate textural maturity and low compositional maturity.
2) Intergranular and intragranular dissolved pores are the predominant pore spaces of reservoir sandstones, while primary pores rarely occur. Lamellar throats and microfractures are the main types of pore throats. Fractures develop poorly in the study area, but relatively well in the eastern Block B. In general, the Lower–Middle Jurassic reservoirs can be classified as pore–dominated sandstone reservoirs with limited fractures, mainly characterized by very low porosity and permeability.
3) Reservoir evolution of the Lower–Middle Jurassic strata is jointly controlled by sedimentation, diagenesis, and tectonic movements. Strong mechanical compaction is observed wildly in the study area, due to the poor compressive strength of reservoir rocks in the central area, deep maximum burial depth of the strata in the eastern area, and the destructive subsidence style in the whole

region. Primary pores are almost entirely destroyed by mechanical compaction. Since the beneficial lithofacies for reservoir evolution such as subaqueous distributary channels and mouth bars develop primarily in the lower section of the strata, and eogenetic calcite cements present intensively at the top of the strata, reservoir pore spaces of the upper section are worse than that of the lower section. Besides, ferroan dolomite cements and quartz overgrowths occupied the remaining intergranular pores furtherly in diagenetic stage. However, lithic and feldspar framework grains as well as authigenic quartz cements are dissolved at different extents by formation dissolution fluids, and dissolved pores are generated largely during the process. The influences of authigenic clay minerals on residual pores and throats are limited due to their low contents. The Neogene–Quaternary tectonic movements caused intensive lateral compressional stress from the southeast, thus made further damage to reservoir pore structure. Nonetheless, fractures generated by tectonic movements (mainly in the eastern Block B) increase reservoir permeability and provide valid percolation pathways for the late dissolution fluids, therefore improve reservoir physical properties obviously.

4) In conclusion, reservoir quality of the Lower–Middle Jurassic strata is generally poor in the study area, but sandstone reservoirs which develop in subaqueous distributary channel and mouth bar lithofacies, and are improved remarkably by dissolution and tectogenetic fractures in the eastern Block B have comparatively high quality, therefore, can be considered as the risk exploration targets in the study area.

Acknowledgements During the course of this work, we benefited from helpful discussions with Prof. Luo Qihou and Prof. Zhang Yinben on sedimentation and diagenesis. We would also like to thank Zhou Keming for the timely help of taking the latest drilling core samples from Turkmenistan.

References

Andrew H, Paul HN (1995) Clay microporosity in reservoir sandstones: an application of quantitative electron microscopy in petrophysical evaluation. AAPG Bull 79(4):563–573

Baojia H, Xianming X, Dongsheng C, Wilkins RWT, Mingquan L (2011) Oil families and their source rocks in the Weixinan Sub–basin, Beibuwan Basin, South China Sea. Org Geochem 42(2011):134–145

Bing Z, Rongcai Z, Henian L, Lei W, Renjin C (2010) Characteristics of carbonate reservoir in Callovian–Oxfordian of Samandepe Gas field, Turkmenistan. Acta Geol Sin 84(1):117–126 (in Chinese with English abstract).

Ehrenberg SN (1993) Preservation of anomalously high porosity in deeply buried sandstones by Grain–coating chlorite: example from the Norwegian continental shelf. AAPG Bull 77(7):1260–1286

Gary N (2014) Sedimentology and stratigraphy (the second edition). Wiley–Blackwell: 280–281.

Guohua Z, Jianfeng S, Zhanguo L, Shaoyi W, Xin W (2012) Atlas of clastic reservoir rocks. Petroleum Industry Press: 97 (in Chinese).

Hailiang C, Rongcai Z, Qiang W (2015) Characteristics of lower–middle Jurassic sandstone reservoirs in Amu Darya Basin, Turkmenistan. Oil Gas Geol 36(6):985–993 (in Chinese with English abstract)

Haowu L, Xiaoguang T, Suhua W, Xiaokang G, Zhixin W, Jianyu G (2010) An analysis of geological characteristics and exploration potential of the Jurassic play, Amu Darya Basin. Nat Gas Ind 30(5):6–12 (in Chinese with English abstract).

Henian L, Minmin D, Lei W, Benquan Z, Xingyang Z, Huaiyi F (2013) Exploration and development of giant carbonate gas field in the Amu Darya right bank area. Science Press: 1–6 (in Chinese).

Jianfeng S, Guohua Z (1998) Study on quantitative prediction of porosity preservation in sandstone reservoirs. Sci Geol Sin 33(2):244–250 (in Chinese with English abstract).

Jianfeng S, Huiliang Z, Yang S, Xin W, Guohua Z, Chunsong S (2006) Diagenetic mechanisms of sandstone reservoirs in China oil and gas–bearing basin. Acta Petrol Sin 022(08):2165–2170 (in Chinese with English abstract).

Jianliang X, Cheng X, Lei W, Huaiyi F, Changnian D (2010) Structural evolution and hydrocarbon pooling conditions in the Amu Darya Right Bank Block, Turkmenistan. Nat Gas Ind 30(5):18–20 (in Chinese with English abstract).

Kewen G (1986) The exploration situation and the prospects of continental petroliferous basins in the world. Oil Gas Geol 7(4):433–436 (in Chinese)

Mingda Y, Minghui Y, Zhenxing T, Yinghui W, Xia C, Jinfeng W (2003) Analysis of hydrocarbon distribution in Daqingzijing area of the southern Songliao Basin. Pet Geol Exp 25(3):252–256 (in Chinese with English abstract).

Qiang W, Huaiyi F, Henian L, Xubin C, Lei W, Xingzhi W (2013) Reservoir characteristics of Callovian–Oxfordian in Chashgui area. Amu Darya Basin Lithologic Reservoirs 25(2):41–48 (in Chinese with English abstract).

Qiang W, Ting Z, Huaiyi F (2014) The diagenetic evolution, petrophysical properties and reservoir contributing factors of the Middle–Lower Jurassic sandstones in Amu Darya right bank area. Research Report: 43-45 (in Chinese).

Quanli S, Hansen S, Bao J, Jianjun Y, Wenjun L (2012) Genesis of chlorites and its relationship with high–quality reservoirs in the Xujiahe Formation tight sandstones, western Sichuan depression. Oil Gas Geol 33(5):751–757 (in Chinese with English abstract).

Robert LF (1968) Petrology of sedimentary rocks. Hemphill Publishing Company, Austin, Texas: 170.

Rongcai Z, Yanghui P, Can Z, Lei W, Renji C, Yang R (2013) Carbon and oxygen isotope stratigraphy of the Oxfordian carbonate rocks in Amu Darya basin. J Earth Sci 24(1):42–56

Shikuo L, Zihe B, Junsheng Y (2013) Structural deformation of the Lower–middle Jurassic series and their trap characteristics in Amu Darya right bank area. Geoscience 27(4):774–782 (in Chinese with English abstract).

Shilei L, Rongcai Z, Wenquan Y, Jun L, Hao J, Xiaoping W (2012) Characteristics of Oxfordian carbonate reservoir in Agayry area, Amu Darya Basin. Lithologic Reservoirs 24(1):57–63 (in Chinese with English abstract).

Sijing H, Wei S, Peipei H, Hongpeng T, Lihong L (2009) The origin of authigenic illite and its effects on reservoir quality: a case study from Taiyuan sandstone, eastern Ordos Basin. J Mineral Petrol 29(4):25–32 (in Chinese with English abstract).

Ting Z, Qiang W, Liu B (2014) Sedimentary facies and its lateral distribution of the Middle–Lower Jurassic in Amu Darya right bank area. Journal of Southwest Petroleum University 36(6):27–38 (in Chinese with English abstract)

Wanbin M, Zhengxiang L, Mingshi F, Shihua Z, Min L, Fahai M (2011) The origin of authigenic illite in tight sandstones and its effect on the formation of relatively high–quality reservoirs: a case study on

sandstones in the 4th member of Xujiahe Formation, western Sichuan Basin. Acta Pet Sin 32(5):783–790 (in Chinese with English abstract).

Wenli X, Rongcai Z, Huaiyi F, Qiang W, Lei W (2012) The sedimentary facies of Callovian–Oxfordian in Amu Darya basin, Turkmenistan. Geol China 39(4):954–963 (in Chinese with English abstract).

Xiaomin Z (2008) Sedimentary petrology (the 4th edition). Petroleum Industry Press: 282–298 (in Chinese).

Xin H, Yanxia J, Shuguang H (2016) Research process of authigenic kaolinite in the sandstone reservoir. Sino–Global Energy 21(3):31–40 (in Chinese with English abstract).

Xinghe Y (2010) Oil and Gas Reservoir Geology. Petroleum Industry Press (in Chinese).

Yan S (2013) The Plays' Characteristics of Petroliferous Basins in Central Asia. Dissertation, China University of Geosciences (in Chinese with English abstract).

Yan D, Qiang W, Xubin C, Lei W, Changcheng Z, Renjin C (2011) Origin and distribution laws of H_2S in carbonate gas reservoirs in the Right Bank Block of the Amu Darya River. Nat Gas Ind 31(4):21–23 (in Chinese with English abstract).

Yu Z, Yachun W, Hui Z, Deping Z, Guohui W (2010) Characteristics of sedimentary micro facies and sand bodies in Qing 2 formation of Daqingzijing area, Songliao Basin. Special Oil and Gas Reservoirs 17(1):54–56 (in Chinese with English abstract).

Yudan H, Chunguang W (2014) Tectonic evolution and its vital role for oil and gas reservoir in Amu Darya Basin. Prog Geophys 29(3): 1143–1147 (in Chinese with English abstract).

Zhijun W, Hongjun T, Fengshan A (2003) Causes of laminae fractures of tight sand gas reservoir in Xinchang, West Sichuan region. Pet Explor Dev 30(2):109–111 (in Chinese with English abstract).

Zhiyong G, Jinggang C, Jiarui F, Zhong L, Xianying H, Xiaopei L, Xuesong Z, Meili G (2013) An effect of burial compaction on deep reservoirs of foreland basins and its reworking mechanism. Acta Pet Sin 34(5):867–876 (in Chinese with English abstract).